Polymorphism at Residue 129 Modulates the Conformational Conversion of the D178N Variant of Human Prion Protein 90−231†

Adrian C. Apetri,‡ David L. Vanik,‡ and Witold K. Surewicz*

Department of Physiology and Biophysics, Case Western Reserve University, Cleveland, Ohio 44106

Received July 25, 2005; Revised Manuscript Received October 3, 2005

ABSTRACT: One of the arguments in favor of the protein-only hypothesis of transmissible spongiform encephalopathies is the link between inherited prion diseases and specific mutations in the *PRNP* gene. One such mutation (Asp178 → Asn) is associated with two distinct disorders: fatal familial insomnia or familial Creutzfeldt−Jakob disease, depending upon the presence of Met or Val at position 129, respectively. In this study, we have characterized the biophysical properties of recombinant human prion proteins (huPrP90−231) corresponding to the polymorphic variants D178N/M129 and D178N/V129. In comparison to the wild-type protein, both polymorphic forms of D178N huPrP show a greatly increased propensity for a conversion to β-sheet-rich oligomers (at acidic pH) and thioflavine T-positive amyloid fibrils (at neutral pH). Importantly, the conversion propensity for the D178N variant is strongly dependent upon the M/V polymorphism at position 129, whereas under identical experimental conditions, no such dependence is observed for the wild-type protein. Amyloid fibrils formed by wild-type huPrP90−231 and the D178N variant are characterized by different secondary structures, and these structures are further modulated by residue 129 polymorphism. Although on the basis of only *in vitro* data, this study strongly suggests that polymorphism-dependent phenotypic variability of familial prion diseases may be linked to differences in biophysical properties of prion protein variants.

Prion diseases or transmissible spongiform encephalopathies (TSEs)[1] are a group of fatal neurodegenerative disorders that affect humans and animals (*1*−*5*). The human forms encompass Creutzfeldt−Jakob disease (CJD), Gerstmann−Straussler−Scheinker disease (GSS), fatal familial insomnia, and kuru, whereas the animal diseases include scrapie in sheep, bovine spongiform encephalopathy in cattle, and chronic wasting disease in elk and deer. The human diseases are unique in that they may arise sporadically, be inherited, or acquired through the exposure to infectious prions. Regardless of the primary etiology, these diseases are associated with the conversion of the cellular prion protein, PrP^{C}, into a misfolded form, PrP^{Sc} (*1*−*7*). This conversion occurs by a post-translational process that appears to involve no covalent modifications (*8*). PrP^{Sc} can be distinguished biochemically from PrP^{C} by its increased resistance to proteinase K digestion, insolubility in nonionic detergents, and a very strong tendency to aggregate into insoluble plaques (*1*−*7*, *9*). In many cases, these aggregates have characteristics of amyloid fibrils. Furthermore, spectroscopic data indicate that PrP^{C} is rich in α-helix structure, whereas PrP^{Sc} is characterized by a relatively high content of β-sheet structure (*10*−*12*).

According to the "protein-only" hypothesis (*1*, *13*), the transmission of prion diseases does not require nucleic acids, and PrP^{Sc} itself is the infectious pathogen that self-propagates by a mechanism involving binding to cellular prion protein and catalyzing its conversion to the PrP^{Sc} state. The molecular details of this conformational conversion remain poorly understood. Nevertheless, the central role of PrP^{Sc} in the disease propagation and pathology is supported by a wealth of biochemical and genetic data (*1*−*7*, *14*). In a more general context, the notion that proteins can act as infectious agents that replicate by self-perpetuating conformational conversion is strongly supported by recent studies on protein-based inheritance in yeast and fungi (*15*−*17*).

In addition to biochemical data, the key piece of evidence supporting the protein-only hypothesis of TSEs is the link between familial prion diseases and mutations in the gene encoding human prion protein. Over 20 such mutations have been shown to date to segregate with familial CJD, GSS disease, or fatal familial insomnia (*1*, *2*, *18*). The pathogenic process in individuals carrying these mutations seems to develop spontaneously. Importantly, some cases of familial CJD and GSS have been successfully transmitted to experimental animals, providing a rationale for a unified description of genetic and infectious forms of prion diseases within the framework of the protein-only model (*18*). In addition to pathogenic mutations, the susceptibility to and the phenotype of prion diseases is strongly dependent upon the M/V

† This work was supported by National Institutes of Health Grants NS 44158 and NS 38604 (to W.K.S.).

* To whom correspondence should be addressed: Department of Physiology and Biophysics, Case Western Reserve University, 10900 Euclid Avenue, Cleveland, OH 44106. Telephone: 216-368-0139. Fax: 216-368-1693. E-mail: wks3@case.edu.

‡ These authors contributed equally to this work.

[1] Abbreviations: TSE, transmissible spongiform encephalopathy; CJD, Creutzfeldt−Jakob disease; GSS, Gerstmann−Straussler−Scheinker disease; GdnHCl, guanidine hydrochloride; PrP, prion protein; PrP^{C}, cellular PrP isoform; PrP^{Sc}, scrapie PrP isoform; huPrP90−231, recombinant human prion protein fragment 90−231; AFM, atomic force microscopy; CD, circular dichroism; FTIR, Fourier transform infrared; ThT, thioflavine T.

10.1021/bi051455+ CCC: $30.25
Published on Web 11/09/2005

polymorphism at residue 129 (*1*, *2*, *18*−*22*). The molecular basis of these effects is, however, unknown. A detailed understanding of how disease-associated mutations and residue 129 polymorphism affect the structure and biophysical properties of prion protein is of fundamental importance, because it may provide clues regarding the mechanism of prion propagation as well as the molecular basis of phenotypic variability of TSEs. Of particular interest in this respect is the D178N mutation. Depending upon the M/V polymorphism, this mutation segregates with two distinct disorders: fatal familial insomnia or familial CJD (*23*). Here, we describe the effect of the D178N substitution and residue 129 polymorphism on the biophysical properties and conformational conversion of human prion protein.

EXPERIMENTAL PROCEDURES

Plasmid Construction and Protein Purification. The plasmid encoding huPrP90−231 with a N-terminal linker containing polyhistidine tag and a thrombin cleavage site was described previously (*24*). The D178N huPrP90−231 variants with methionie 129 and valine 129 were constructed by site-directed mutagenesis using a Quick Change kit and the appropriate primers. All proteins were expressed, digested with thrombin, and purified according to the previously reported protocol (*24*, *25*). The concentration of proteins was determined spectrophotometrically using the molar extinction coefficient (ϵ_{276}) of 21 640 M^{-1} cm^{-1}. The purified protein was dialyzed against 10 mM acetate buffer at pH 4.0, concentrated to approximately 5 mg/mL, and stored at −80 °C. In our experience, PrP90−231 in acetate buffer has very little tendency to self-associate. Nevertheless, to remove any potential aggregates, immediately before each experiment, the protein solution was centrifuged for 20 min at 15000*g*, followed by filtration through a 100-kDa cutoff membrane. Analysis by dynamic light scattering (Dyna Pro; Protein Solutions, Inc.) confirmed that the protein prepared in this manner was monomeric, with no detectable presence of high-molecular-weight oligomers.

Conversion to Oligomeric β-Sheet Structure at Acidic pH. The proteins from a stock solution described above were transferred to 50 mM sodium acetate buffer containing 1 M GdnHCl at pH 5.0 (final protein concentration of 60 or 150 μM) and incubated without agitation at 25 °C. The α-helix → β-sheet transition was monitored by far-UV circular dichroism (CD) spectroscopy using an AVIV 215 spectropolarimeter and a 0.2 mm path-length cell. The progress of protein oligomerization was followed by analytical size-exclusion chromatography on a Bio-Sil SEC-250 column (Bio-Rad) as described previously (*26*).

Conversion to Amyloid Fibrils at Neutral pH. The proteins from a stock solution were diluted to a final concentration of 50 μM in 50 mM Tris-HCl buffer at pH 7.5, without or in the presence of 1 or 2 M GdnHCl. The samples were placed in 1.5 mL conical tubes filled to the volume of 0.8 mL and incubated at 37 °C with continuous rotation at 8 rpm (Barnstead Thermolyne Labquake rotator). The formation of amyloid fibrils was followed by a fluorometric thioflavine T (ThT) assay (*27*). To this end, 5 μL aliquots of each sample were withdrawn at different time points and transferred to a quartz cell containing 10 μM ThT in 50 mM phosphate at pH 6.4. After 30 s of incubation, the fluorescence of ThT was measured at 482 nm upon excitation at 450 nm. The final protein concentration in the ThT buffer was 0.5 μM. The lag phases reported in the text represent average values based on 3−4 independent experiments.

Fourier Transform Infrared (FTIR) Spectroscopy. Samples for infrared spectroscopy were converted to amyloid fibrils as described above. Because H_2O and GdnHCl have very strong absorbance in the amide I region and thus interfere with FTIR measurements, the aggregated protein was then washed several times with D_2O by low-speed centrifugation in an Eppendorf centrifuge. Samples were placed between two calcium fluoride windows separated by a 50-μm Teflon spacer, and FTIR spectra were obtained at room temperature on a Bruker IFS 66 instrument. For each spectrum, 256 scans were collected and Fourier-transformed to give a resolution of 2 cm^{-1}. Spectra were corrected for residual absorption of buffer by interactively subtracting the spectrum of buffer alone until a flat baseline was obtained between 1700 and 1850 cm^{-1}. Overlapping bands in the amide I region were resolved by Fourier self-deconvolution (*28*) in the Opus 4.0 software package, using a Lorentzian band shape and parameters equivalent to a 15 cm^{-1} half-width and a resolution enhancement factor of 1.6.

Atomic Force Microscopy (AFM). The converted (oligomeric) protein samples were applied to a freshly cleaved mica substrate. After 30 s, the surface was extensively rinsed with ultrapure water to remove salts and unbound protein. The preparation was then dried in a stream of nitrogen and mounted on a microscope scanner. The images were recorded in a tapping mode on a Digital Instruments Multimode atomic force microscope equipped with Nanoscope IV controller and a type E scanner. All images were acquired using single-beam silicon probes with a nominal spring constant of 40 N/m and nominal tip radius of 10 nm. Data were processed by interactive planefitting and Gaussian low-pass filtering using the Nanoscope SPM software package. Average fibril height and axial periodicity were measured from processed AFM height images using Nanoscope offline analysis routines (*29*).

Equilibrium Unfolding in Urea. The urea-induced unfolding curves were obtained using an AVIV 215 CD spectrometer equipped with an automatic titrator and a Peltier temperature control system. The measurements were carried out at 25 °C in 50 mM sodium acetate buffer at pH 5.0 or 100 mM Tris-HCl buffer at pH 7.0. Native protein (1.4 μM) in one of the above buffers was titrated, using urea increments of 0.1−0.2 M, with a 9 M buffered urea solution of identical protein concentration. Upon each addition of urea, the mixture was incubated for 15 s and the extent of protein unfolding was monitored by changes in ellipticity at 222 nm. The unfolding curves were analyzed using a two-state transition model as described previously (*30*). Earlier studies have shown that the unfolding/refolding of the prion protein is fully completed within milliseconds and that the unfolding and refolding reactions are fully reversible (*31*, *32*). The urea used in this study was deionized by treatment with a mixture of anion-exchange (trimethylbenzylammonium) and cation-exchange (Dowex MR-3) resins. The concentration of the denaturant was determined by refractive index measurements.

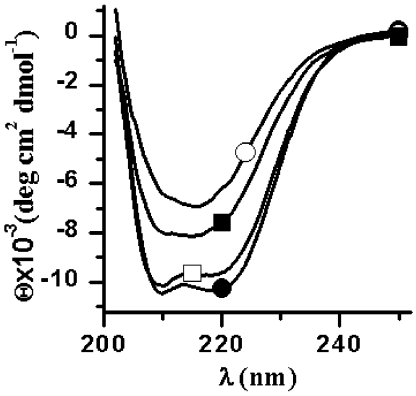

FIGURE 1: Time-dependent transition of huPrP90−231 to the β-sheet structure at acidic pH as monitored by CD spectroscopy. Spectra for M129 huPrP90−231 (150 μM) in 50 mM sodium acetate buffer at pH 5.0 in the absence of GdnHCl (●) and recorded 2 h (□), 4 h (■), and 10 h (○) after the addition of 1 M GdnHCl.

RESULTS

Previous studies have shown that, depending upon experimental conditions, the recombinant prion protein 90−231 (PrP90−231) can be converted into a variety of oligomeric β-sheet-rich structures with different physicochemical properties. Under mildly acidic conditions (pH 5 or below) in the presence of low concentrations of GdnHCl (or urea and NaCl), the protein forms β-sheet oligomers that show little affinity for ThT dye (*33*−*36*), whereas at neutral pH, it can be converted to highly ThT-positive amyloid structures with fibrilar morphology (*35*, *37*). Here, we have probed the effect of the D178N mutation and residue 129 polymorphism on these two distinct conversion pathways of human prion protein.

Polymorphism-Dependent Conversion to β-Sheet-Rich Oligomers under Acidic Conditions. Consistent with the previous paper (*33*), incubation of huPrP90−231 in 50 mM acetate buffer (pH 5.0) in the presence of 1 M GdnHCl results in a time-dependent transition from the native α-helical form to β-sheet structure. This reaction can be monitored by CD spectroscopy (Figure 1). A similar transition was observed for the D178N variant, although for the latter protein, the reaction occurred within a much shorter time scale. As shown in previous studies (*33*, *34*), the rate of the conversion reaction can be readily followed by monitoring changes in ellipticity at 222 nm. Representative kinetic data at a protein concentration of 60 μM are shown in Figure 2A. These data clearly shows that the conversion rate for D178N huPrP90−231 strongly depends upon the polymorphism at residue 129; it is approximately 6 times faster for the M129 polymorph than for the V129 polymorph (apparent half times of 22 ± 5 and 130 ± 10 min, respectively). Analogous to previous observations for the wild-type huPrP90−231 (*33*, *34*) and the F198S mutant (*26*), the α-helix → β-sheet transition for D178N variants was invariably associated with protein oligomerization. Indeed, when followed by size-exclusion chromatography, the kinetics of oligomer formation by the D178N/V129 variant (as assessed by monitoring the decrease in the area of the peak corresponding to the protein monomer) was indistinguishable from that of changes in CD spectra (Figure 2A). Detailed kinetic analysis of oligomer formation by size-exclusion chromatography for the D178N/129M polymorph was not feasible because of a much faster rate

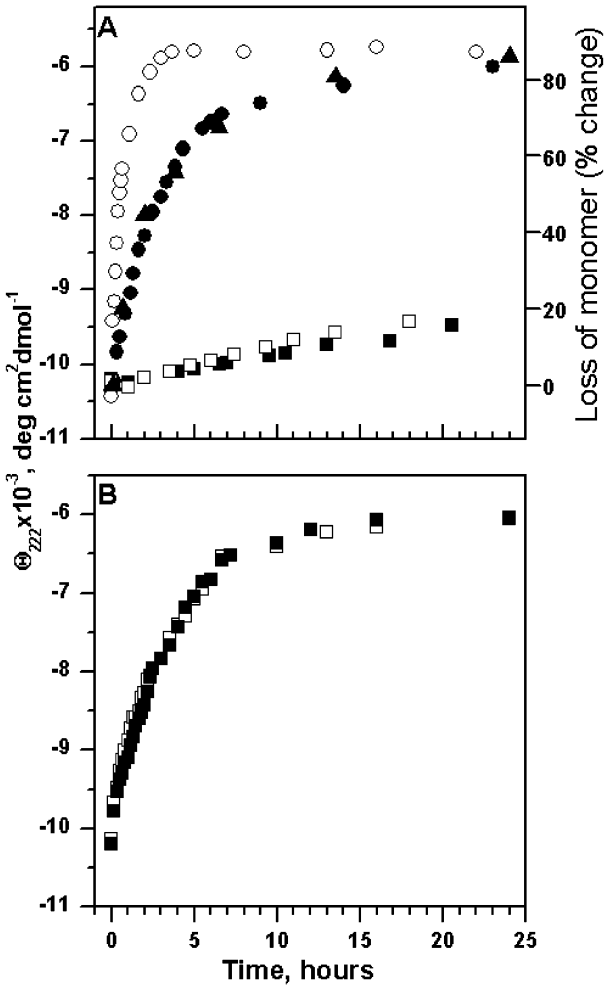

FIGURE 2: Time course of the α-helix → β-sheet transition for huPrP90−231 variants in the presence of 1 M GdnHCl at pH 5.0. (A) Time course of conformational transition for D178N/M129 variant (○), D178N/V129 variant (●), wild-type with M129 polymorphism (□), and wild-type with V129 polymorphism (■) as followed by changes in ellipticity at 222 nm at a protein concentration of 60 μM. The apparent half-times of the reaction, on the basis of three independent experiments, are 22 ± 5 and 130 ± 10 min for the D178N/M129 and D178N/V129 variants, respectively. (▲) Kinetics of D178N/V129 huPrP90−231 oligomerization as monitored by size-exclusion chromatography. The percent decrease in the area of the peak corresponding to the protein monomer is plotted as a function of the incubation time (right axis). (B) Time course of conformational transition for the M129 (□) and V129 (■) polymorphs of wild-type huPrP90−231 at increased protein concentrations of 150 μM. The reaction was followed by changes in ellipticity at 222 nm. The apparent half-times of the reaction, on the basis of three independent experiments, are 115 ± 12 and 110 ± 15 min for the M129 and V129 polymorphs, respectively.

of the reaction. Nevertheless, the rapid drop in the intensity of the monomeric peak was fully consistent with the CD data.

Under identical experimental conditions (pH 5, 1 M GdnHCl, protein concentration of 60 μM), the conversion rate for the wild-type huPrP90−231 was much slower than that for the D178N variant, with little changes in CD spectra seen even after 24 h of incubation (Figure 2A). To assess whether the M/V polymorphism at residue 129 affects in a similar manner the conversion rate of the wild-type huPrP, experiments for the latter protein were repeated at a higher protein concentration, i.e., under the conditions expected to

accelerate the rate of the reaction (*33*, *34*). Indeed, at a protein concentration of 150 μM, wild-type huPrP90−231 converted to β-sheet-rich aggregates within several hours (Figure 1). However, in sharp contrast to the D178N variant, the reaction rates for the wild-type protein were essentially identical for both polymorphic forms, regardless of the nature of the amino acid residue at position 129 (apparent half-times of 115 ± 12 and 110 ± 15 min for the M129 and V129 polymorph, respectively; Figure 2B). Thus, while the M/V polymorphism at position 129 strongly modulates the α-helix → oligomeric β-sheet conversion of D178N huPrP90−231, it appears to have no effect on this conversion in the absence of the D178N mutation.

Polymorphism-Dependent Conversion to Amyloid Fibrils at Neutral pH. Prompted by the observations under mildly acidic conditions, we next examined the effect of residue 129 polymorphism on the conversion propensity and biophysical properties of D178N huPrP90−231 at neutral pH. Incubation of both polymorphic variants of the D178N mutant (protein concentration of 50 μM) at 37 °C in 50 mM Tris-HCl buffer at pH 7.5 for a period of 3−4 days resulted in a gradual aggregation and precipitation of the protein. These aggregates appeared in electron micrographs as largely amorphous structures and, when examined by fluorescence spectroscopy, showed very little affinity for the ThT dye. However, upon incubation in the same buffer with gentle rotation (8 rpm), a time-dependent increase in ThT fluorescence was observed, indicating that under the latter conditions the protein self-assembles into amyloid-like structures. Importantly, in contrast to β-sheet-rich oligomers formed at mildly acidic pH, the kinetic curves for the assembly of ThT-positive structures were characterized by well-defined lag and growth phases (Figure 3A), with the features typical for a nucleation-dependent polymerization reaction (*38*). Similar to the polymorphism-dependent conformational transition of D178N huPrP90−231 at acidic pH, also the conversion of the mutant protein to amyloid structures (at neutral pH) was much faster for the M129 polymorph than for the V129 variant (lag phases under present experimental conditions of 14 ± 2 and 30 ± 3 h, respectively). It should be noted that the formation of ThT-positive structures at neutral pH was accompanied by a substantial increase in sample turbidity. This precluded CD measurements similar to those described for the conformational transition at acidic pH.

Under identical experimental conditions (50 mM Tris-HCl buffer at pH 7.5; protein concentration of 50 μM), wild-type huPrP90−231 was much less prone to convert to amyloid structures, with no ThT response seen even after 150 h of incubation (Figure 3B). Therefore, under these experimental conditions, we could not assess whether the 129 M/V polymorphism has any effect on the conversion of the wild-type human prion protein. However, such a comparison became feasible when experiments were performed in a buffer containing denaturing agents such as GdnHCl. As shown in Figure 3C, analogous to the trend observed in a denaturant-free buffer, the conversion rate for D178N huPrP90−231 in the presence of 1 M GdnHCl is approximately 2-fold faster in the case of the M129 polymorph than the V129 polymorph (lag phases of 4.5 ± 0.5 and 9.2 ± 0.8 h). However, in contrast to the mutant protein, residue 129 polymorphism has no effect on the conversion rate of the wild-type huPrP90−231, with both polymorphic forms showing essentially identical lag phases of 22 h (Figure 3D).

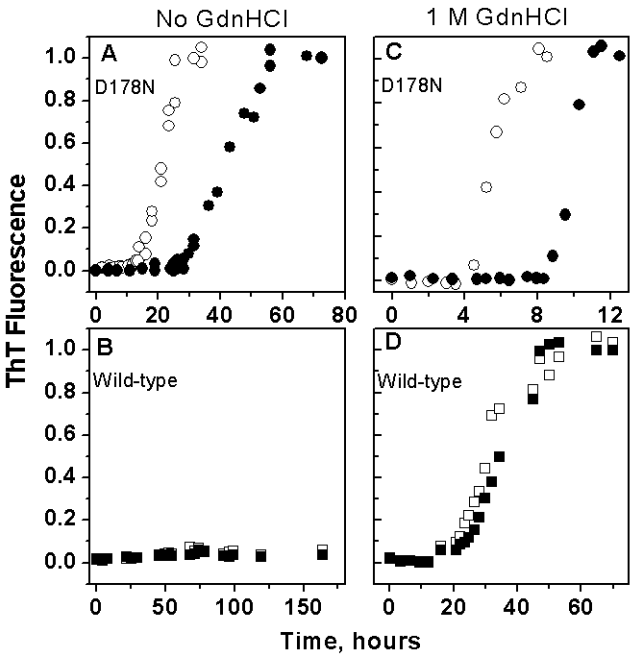

FIGURE 3: Time course of amyloid fibril formation for huPrP90−231 variants as monitored by ThT fluorescence. (A and C) D178N huPrP90−231 with M129 (○) and V129 (●). (B and D) Wild-type huPrP90−231 with M129 (□) and V129 (■). The proteins (50 μM) were incubated at 37 °C under the condition of gentle rotation (8 rpm) in 50 mM Tris-HCl buffer at pH 7.5 in the absence of any denaturant (A and B) and in the presence of 1 M GdnHCl (C and D). Data are expressed as a fraction of the maximal ThT fluorescence increase in a given experiment. Under the present experimental conditions (final protein concentration of 5 μM in 50 mM potassium phosphate buffer, containing 10 μM ThT at pH 6.4), we typically observed a 20−30-fold increase in the ThT fluorescence. The lag phases of the conversion reaction in the absence of GdnHCl (A) are 14 ± 2 and 30 ± 3 h for the D178N/M129 and D178N/V129 variants, respectively. In the presence of 1 M GdnHCl (C), the lag phases for these two variants are 4.5 ± 0.5 and 9.2 ± 0.8 h, respectively. The lag phases for the conversion of wild-type huPrP90−231 with M129 and V129 polymorphisms are 22 ± 2 and 22 ± 3 h, respectively (D). These lag phases and standard deviation values are based on 3−4 independent experiments.

Structural Characteristics of PrP90−231 Amyloid Fibrils. The morphology of the self-assembled ThT-positive structures formed by D178N huPrP90231 was examined by AFM. AFM images of protein converted under the conditions of mild rotation (8 rpm) at neutral pH in the presence of GdnHCl revealed the network of well-separated amyloid fibrils. These fibrils are of variable length and have an average height of 5−6 nm (Figure 4A). Higher magnification images of individual fibrils clearly show an axial periodicity of 70−80 nm (Figure 4B). Within the resolution limits of our AFM measurements, no significant morphological differences were seen between the fibrils formed by two different polymorphic variants of D178N huPrP90−231. It should be noted that protein samples converted to ThT-positive structures in the absence of the denaturant had a very strong tendency to clump into large aggregates; this precluded acquisition of high-quality AFM images.

The secondary structure of oligomers formed by polymorphic variants of huPrP90−231 at neutral pH was probed by FTIR spectroscopy. This method is especially well-suited for studying aggregated proteins because high-quality FTIR

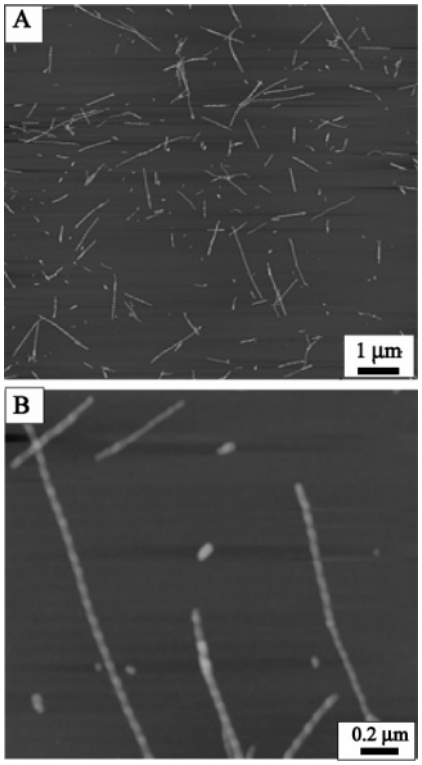

FIGURE 4: AFM images of D178N/M129 huPrP90−231 amyloid fibrils. (A) Low magnification image illustrating the abundance and length variability of fibrils. (B) High-magnification image of individual fibrils. Identical fibrils were observed for D178N/V129 huPrP90−231. Fibrils were obtained upon incubation of the protein at 37 °C in 50 mM Tris-HCl buffer containing 2 M GdnHCl.

spectra can be acquired for light-scattering samples and the spectra are very sensitive to β-sheet structures. The positions of infrared amide I bands associated with these structures depend upon many factors, including the strength of hydrogen bonds and molecular packing of β strands (*28*, *39*, *40*). Figure 5 shows original FTIR spectra for D178N/M129 huPrP90−231 in a native monomeric form and in two different aggregated states. Consistent with previous data for the wild-type protein (*26*), the spectrum of a freshly prepared sample of monomeric D178N/M129 variant has a maximum at 1648 cm^{-1}, characteristic of a native α-helix-rich conformation. An identical spectrum was observed for the V129 polymorphic form (not shown for brevity). Upon 2−3 days of incubation at 37 °C under nonperturbing conditions (no rotation), the FTIR spectrum of the aggregated protein was quite different, showing two well-resolved bands at 1620 and about 1640 cm^{-1}. Another spectrum, characterized by a maximum at 1625 cm^{-1} and a shoulder around 1662 cm^{-1}, was observed upon protein conversion to ThT-positive amyloid fibrils (incubation with a gentle rotation). Both the 1620 and 1625 cm^{-1} bands are characteristic of β sheets (*28*, *39*, *40*). However, different positions of these bands clearly indicate nonequivalence in molecular organization of β strands in the ThT-negative and ThT-positive D178N huPrP90−231 aggregates.

To explore whether the secondary structure of amyloid fibrils is affected by the M/V polymorphism at residue 129, FTIR spectra were further analyzed using the procedure of band narrowing by Fourier self-deconvolution. This mathematical procedure increases the resolution of overlapping bands that contribute to broad amide I contours (*28*). To

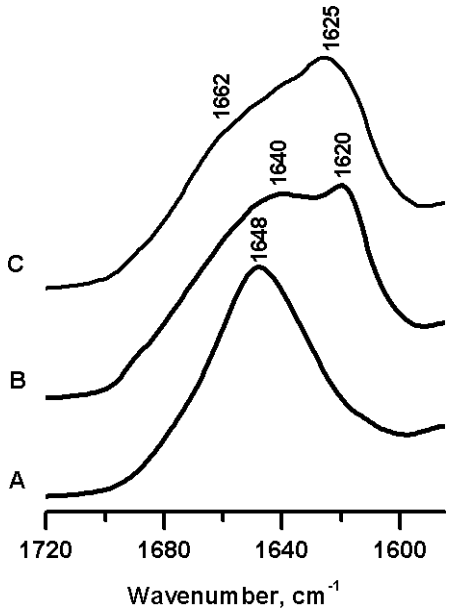

FIGURE 5: Infrared spectra of different forms of D178N/M129 huPrP90−231. (A) Monomeric protein. (B) Aggregated protein after 3 days of incubation at 37 °C under nonperturbing conditions (no rotation) in 50 mM Tris-HCl buffer at pH 7.5. (C) Fibrilar form of the protein after 2 days of incubation at 37 °C with gentle rotation (8 rpm) in 50 mM Tris-HCl buffer at pH 7.5.

allow direct comparison of fibrils formed by D178N and wild-type huPrP90−231, this analysis was performed on spectra of proteins converted in the presence of 1 M GdnHCl. As shown in Figure 6A, deconvolved spectrum of the D178N/M129 variant shows a major band at 1627 cm^{-1} and additional relatively well-resolved bands at 1650 and 1662 cm^{-1}. The 1627 cm^{-1} band is highly characteristic of the β-sheet structure, whereas bands at 1650 and 1662 cm^{-1} likely correspond to the α-helix structure and turns, respectively (*28*, *39*). The spectrum of the V129 polymorph of D178N huPrP90−231 is somewhat different, with a major β-sheet band shifted to 1628 cm^{-1} and the α-helical band at 1652 cm^{-1}. Furthermore, the spectrum of the M129 polymorph shows an additional band at 1638 cm^{-1}. The latter band, missing in the spectrum of the V129 polymorph, is also in the frequency range usually assigned to β structure (*28*, *39*). Although small, the spectral differences depicted in Figure 6A were highly reproducible in many independent experiments (i.e., bands in the spectra recorded for multiple samples of each protein were always present at the same position), indicating subtle differences in the secondary structure of fibrils formed by the two polymorphic forms of the D178N mutant of human prion protein.

Fourier self-deconvolved spectra of fibrils formed by the wild-type protein (Figure 6B) were substantially different from those of D178N huPrP90−231 amyloids, with a major β-sheet band appearing at a considerably lower wavenumber (1622/1623 cm^{-1}). The frequency of this band was slightly (one wavenumber) lower for the M129 polymorph than for the V129 polymorph.

pH-Dependent Thermodynamic Stability of the Wild-Type and D178N Variants of huPrP90−231. The thermodynamic stability of huPrP90−231 variants was studied by equilibrium unfolding in urea (Figure 7). In contrast to GdnHCl at acidic pH, urea under present experimental conditions does not promote the conversion of prion protein to oligomeric β-sheet

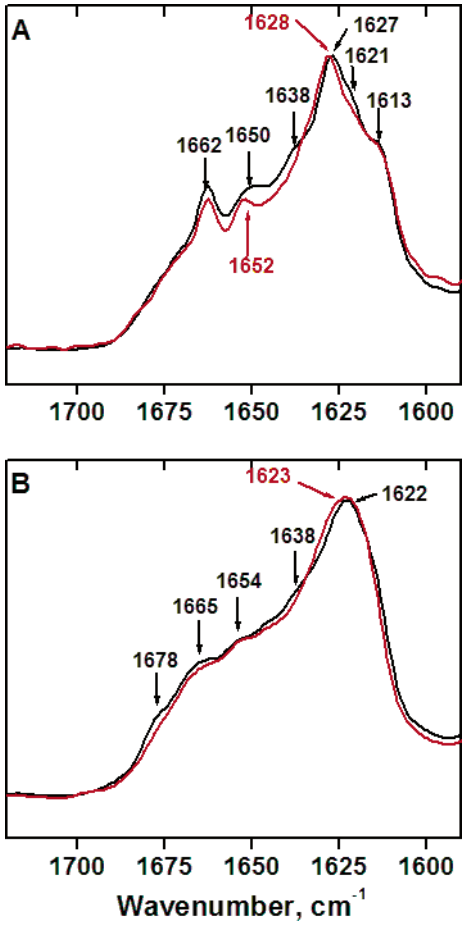

FIGURE 6: Infrared spectra after band narrowing by Fourier self-deconvolution for fibrillar (ThT-positive) forms of D178N variants (A) and wild-type huPrP90−231 (B). Black traces, variants with M129; Red traces, variants with V129. Proteins were converted to amyloid fibrils in 50 mM Tris-HCl buffer and 1 M GdnHCl at pH 7.5. All spectra were Fourier-deconvolved using identical parameters as described in the Experimental Procedures.

structure (*31*, *41*−*43*). The unfolding curves in urea show no dependence on the protein concentration, indicating that the protein stays monomeric throughout the unfolding process (*44*). Thus, as shown in a number of previous studies (*31*, *41*−*43*), this denaturant is well-suited for probing the thermodynamic stability of prion protein and variants thereof.

Although recent kinetic measurements detected an intermediate in prion protein folding (*31*, *44*), the population of this intermediate is well below the detection limit of the present equilibrium experiments. Therefore, equilibrium unfolding data were analyzed according to a two-state transition model, providing information about the global stability (free-energy difference between the native and fully unfolded states) of prion protein variants. As summarized in Table 1, both under neutral (pH 7) and mildly acidic conditions (pH 5), the D178N variants displayed much lower thermodynamic stability than the wild-type huPrP90−231. The present data for huPrP90−231 at neutral pH are consistent with those reported previously for mouse PrP variants (*41*). Under all conditions studied, the unfolding curves were only marginally affected by the nature of the amino acid residue at position 129, indicating that the M/V polymorphism at position 129 has no significant effect on the global thermodynamic stability of the wild-type prion protein or the disease-associated D178N variant (Table 1).

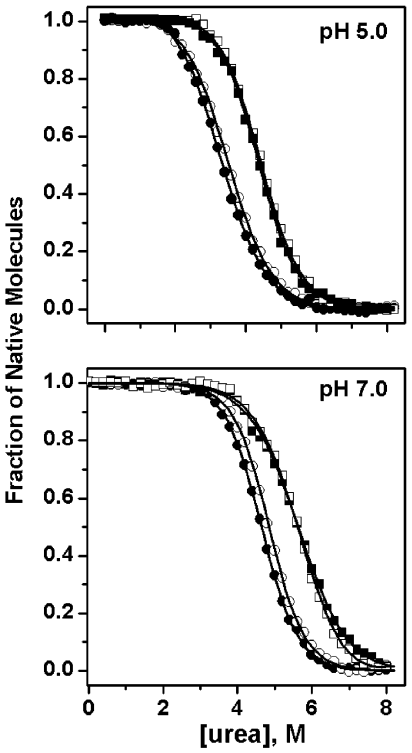

FIGURE 7: Normalized equilibrium denaturation curves in urea for huPrP90−231 variants. (○) D178N/M129 variant, (●) D178N/V129 variant, (□) wild-type with M129, and (■) wild-type with V129. Solid lines represent the best fit of the experimental data to a two-state unfolding model (*30*).

Table 1: pH-Dependent Thermodynamic Stability of Residue 129 Polymorphic Variants of the Wild-Type and D178N huPrP90−231

pH	huPrP90−231 variant	C_m[a] (M)	ΔG[b] (kJ/mol)
5.0	wild-type M129	4.4	18.4 ± 0.5
	wild-type V129	4.3	18.5 ± 0.6
	D178N/M129	3.5	14.7 ± 0.4
	D178N/V129	3.4	14.3 ± 0.5
7.0	wild-type M129	5.6	26.9 ± 0.6
	wild-type V129	5.7	27.2 ± 0.7
	D178N/M129	4.8	24.0 ± 0.6
	D178N/V129	4.7	23.5 ± 0.5

[a] Midpoint unfolding urea concentration. [b] Free-energy difference between the native and unfolded state. The reported mean values and standard deviations are based on three independent experiments.

DISCUSSION

One of the key arguments in favor of the protein-only model of TSEs is the link between mutations in the gene encoding prion protein and familial forms of CJD, GSS, and fatal familial insomnia (*1*−*4*, *18*). Importantly, in contrast to prion diseases acquired by infection, the pathogenic process in individuals carrying these mutations appears to develop spontaneously, i.e., without requiring exogenous PrP^{Sc}. Therefore, understanding how familial mutations affect the mechanism of $PrP^{C} \rightarrow PrP^{Sc}$ conversion should provide important clues regarding the molecular basis of the disease. While it has been originally proposed that familial mutations promote the conversion of the prion protein by decreasing the global thermodynamic stability of PrP^{C} (*45*), direct thermodynamic measurements revealed that many of the disease-associated mutations produce negligible thermodynamic destabilization of the native state relative to the

unfolded state (*41*, *46*). A better correlation was found in a recent study showing that the majority of disease-associated mutations increase the population of monomeric folding intermediates in prion protein folding (*44*). However, the model based on mutation-induced stabilization of partially folded intermediates is also not universal, suggesting that simple thermodynamic concepts cannot explain all hereditary forms of prion disease and that there might be multiple mechanisms by which mutations facilitate the pathogenic process in TSEs (*44*). The molecular nature of these mechanisms remains unknown.

One of the most intriguing disease-related mutations is the aspartic acid to asparagine substitution at position 178. Depending upon the polymorphism at position 129, this mutation leads to different phenotypes of human prion disease; the D178N mutation with Met129 is associated with fatal familial insomnia, whereas the same mutation with Val129 correlates with hereditary CJD (*23*). The Met/Val polymorphism at position 129 is also crucial to the etiology and neuropathology of prion diseases in the absence of the D178N mutation; it is associated with propagation of distinct human prion strains, affects the susceptibility to iatrogenic CJD, and appears to control the susceptibility of humans to variant CJD, a disease believed to be acquired by infection with bovine spongiform encephalopathy (*18*−*22*).

The present study set out to establish whether polymorphism-dependent phenotypic variability of familial prion diseases with the D178N mutation can be correlated with differences in biophysical properties and the conversion propensity of the recombinant prion protein *in vitro*. As a control, we have also examined the effect of residue 129 polymorphism on the behavior of the wild-type prion protein. Like most previous studies with the recombinant prion protein, the experiments were performed using the N-terminally truncated protein encompassing residues 90−231. This region of PrP is of special importance because it encompasses the entire sequence of proteinase K-resistant brain PrP^{Sc}, contains all known point mutations associated with familial prion disorders, and is sufficient for the propagation of the disease. However, most recent data indicates that the aggregation properties of the full-length PrP may be also modulated by the unstructured N-terminal region 23−90 (*47*). The key findings of the present study are (i) in comparison to the wild-type recombinant PrP90−231, the D178N variant is characterized by a greatly increased propensity to undergo a conformational conversion to oligomeric β-sheet-rich forms; (ii) for the D178N variant, the conversion propensity is strongly dependent upon the M/V polymorphism at position 129, whereas no such dependence is observed for the wild-type protein; (iii) amyloid fibrils formed by wild-type huPrP90−231 and the D178N variant are characterized by different secondary structures, and these structures are further modulated by the residue 129 polymorphism.

The experiments described in this study were performed under experimental condition leading to two distinct conversion pathways: one (acidic pH, 1 M GdnHCl, and no agitation) resulting in β-sheet oligomers with little affinity for ThT dye and one (neutral pH and gentle rotation) resulting in ThT-positive amyloid fibrils. It should be noted that the conditions established here for the conversion of the recombinant PrP to amyloid fibrils are significantly different from those described previously by Baskakov et al. (*35*, *37*). While previous experiments required very vigorous shaking (600 rpm) and high concentrations of denaturing agents (*35*, *37*), the conversion of PrP to amyloid structures in this study was accomplished under much milder and thus physiologically more relevant conditions of very gentle rotation (8 rpm) and little or no denaturants. A detailed study describing the mechanism of this autocatalytic conversion is currently in progress.

Regardless of the pathway, the conformational conversion was found to be much faster for the D178N variant than that for wild-type huPrP90−231. This mutation-induced increase in the conversion propensity is similar to the effect reported in our previous study with F198S huPrP, a variant associated with familial GSS (*26*). In both cases, the greater conversion propensity of the mutant proteins could be rationalized within the context of a "thermodynamic model" because both the F198S and D178N substitutions greatly decrease the thermodynamic stability of the native state, increasing the population of the unfolded state as well as that of a partially folded intermediate (*44*).

The most intriguing finding of the present study is that the conversion tendency of the D178N variant of huPrP90−231 is strongly modulated by the polymorphism at position 129, with the M129 polymorph undergoing a much faster conversion than the V129 polymorph. Importantly, under identical experimental conditions, the residue 129 polymorphism did not have any measurable effect on the conversion kinetics of wild-type huPrP90−231. It should be noted that our findings regarding similar fibrillization kinetics of two polymorphic forms of wild-type PrP are generally consistent with recent data of Tahiri-Alaoui and James (*48*), even though these authors used harsher experimental conditions of very vigorous shaking and substantially higher concentrations of denaturing agents.[2] Thus, the polymorphism-dependent differences in the conversion propensity of the D178N variant found in the present study appear to be related to an interplay between residues 178 and 129 and the effect of this interplay on biophysical properties of the prion protein. From the structural perspective, a recent NMR study revealed that the 129 M/V polymorphism has no measurable effect on the native structure of wild-type PrP^{C} (*42*). No high-resolution structural data is yet available for prion protein with the D178N mutation. Riek et al. pointed out that in the wild-type PrP Asp178 forms a salt bridge with Arg164 and a hydrogen bond with Tyr128, a residue sequentially adjacent to position 129 (*49*). These authors also proposed that Asp178-Asn replacement would affect this hydrogen-bonding network differently depending upon the nature of the amino acid residue at position 129, providing a rationale for

[2] In other recent studies, it was reported that, depending upon experimental conditions, the methionine 129 variant of wild-type recombinant human prion protein (with unremoved poly-His tails) aggregates more (*59*) or less (*60*) rapidly than the valine 129 variant. However, all of these observations were made under the conditions of protein refolding from a *fully unfolded state* (6 M GdnHCl) and, in some cases (*59*), at a very high protein concentration (10−30 mg/mL). The present study addresses the effect of residue 129 polymorphism on prion protein conversion to β-sheet oligomers and amyloid fibrils from the physiologically more relevant *native* α*-helical conformation*. Furthermore, the main focus of the present work is on polymorphism-dependent conversion propensity of the disease-associated D178N PrP variant. None of the previous studies dealt with the latter variant.

polymorphism-dependent phenotypic variability of familial prion diseases with the D178N mutation. This is a plausible scenario, consistent with some molecular dynamic simulation studies (*50*−*52*). However, it should be noted that the original model of Riek et al. (*49*) was based on the NMR-derived structure for mouse PrP121−231. Inspection of available NMR data for human prion protein (*53*−*55*) provides less convincing evidence for such a hydrogen-bond network in the latter protein. Clearly, high-resolution NMR or crystallographic data are needed for D178N PrP variants to properly assess the structural consequences of 129 M/V substitution on the background of the D178N mutation. In the absence of direct structural data, any attempts to rationalize the polymorphism-dependent behavior of D178N PrP in terms of specific side-chain and/or backbone interactions remain highly speculative. For example, a recent dynamic simulations study (on the basis of NMR data for the wild-type PrP) concluded that the conversion to β-sheet structure should occur more readily for prion protein with Val129 than for the Met129 variant (*56*). This theoretical prediction is not supported by the present experimental data.

While the atomic-level insight is still missing, it should be noted that the greater conversion propensity of D178N PrP90−231 with Met129 than Val129 as observed in the present study correlates well with recent data on mutation-dependent stability of a monomeric intermediate in prion protein folding (*44*). The population of this intermediate was found to be almost 2-fold higher for D178N/M129 as compared with the D178N/V129 variant. As discussed previously (*31*, *44*), the folding intermediate represents a likely candidate for a direct monomeric precursor of the aggregated state(s) that eventually leads to the pathogenic PrP^{Sc} isoform. In addition to the differences at the level of a monomeric folding intermediate, the effect of residue 129 M/V polymorphism on the phenotype of familial prion disease with the D178N mutation may also be related to polymorphism-dependent differences in the conformation and/or stability of intermediate oligomeric structure(s) on the $PrP^{C} \rightarrow PrP^{Sc}$ conversion pathway or the structure of PrP^{Sc} itself. Indeed, the FTIR data point to conformational nonequivalence of amyloid fibrils formed by D178N huPrP90−231 with Met and Val at position 129. Although the differences in fibril conformation appear very small at the global level reported by infrared spectroscopy, they may be much more substantial at the local level. It is worth noting that the spectral differences between the D178N/M129 and D178N/V129 variants are reminiscent of, although not identical to, those observed previously by Caughey et al. for different strains of hamster PrP^{Sc} (*57*). For example, the infrared spectrum of PrP^{Sc} from the hyper hamster TSE strain is characterized by amide I β-sheet bands at 1626 and 1636 cm^{-1}, whereas the spectrum of the drowsy strain shows a major band at around 1629 cm^{-1}.

A full understanding of the molecular basis underlying polymorphism-dependent variability of prion diseases with the D178N mutation will require further studies, both at the structural and metabolic level (*58*). Nevertheless, the present data strongly suggest that there might be a link between disease phenotype and biophysical properties of polymorphic variants of human PrP, providing a foundation for future work.

REFERENCES

1. Prusiner, S. B. (1998) Prions, *Proc. Natl. Acad. Sci. U.S.A. 95*, 13363−13383.
2. Collinge, J. (2001) Prion diseases of humans and animals: Their causes and molecular basis, *Annu. Rev. Neurosci. 24*, 519−550.
3. Weissmann, C. (2004) The state of the prion, *Nat. Rev. Microbiol. 2*, 861−871.
4. Aguzzi, A., and Polymenidou, M. (2004) Mammalian prion biology: One century of evolving concepts, *Cell 116*, 313−327.
5. Caughey, B., and Chesebro, B. (2001) Transmissible spongiform encephalopathies and prion protein interconversions, *Adv. Virus Res. 56*, 277−311.
6. Caughey, B. (2001) Interactions between prion protein isoforms: The kiss of death? *Trends Biochem. Sci. 26*, 235−242.
7. Priola, S. A. (2001) Prion protein diversity and disease in the transmissible spongiform encephalopathies, *Adv. Protein Chem. 57*, 1−27.
8. Stahl, N., Baldwin, M. A., Teplow, D. B., Hood, L., Gibson, B. W., Burlingame, A. L., and Prusiner, S. B. (1993) Structural studies of the scrapie prion protein using mass spectrometry and amino acid sequencing, *Biochemistry 32*, 1991−2002.
9. Meyer, R. K., McKinley, M. P., Bowman, K. A., Braunfeld, M. B., Barry, R. A., and Prusiner, S. B. (1986) Separation and properties of cellular and scrapie prion proteins, *Proc. Natl. Acad. Sci. U.S.A. 83*, 2310−2314.
10. Caughey, B. W., Dong, A., Bhat, K. S., Ernst, D., Hayes, S. F., and Caughey, W. S. (1991) Secondary structure analysis of the scrapie-associated protein PrP 27−30 in water by infrared spectroscopy, *Biochemistry 30*, 7672−7680.
11. Pan, K. M., Baldwin, M., Nguyen, J., Gasset, M., Serban, A., Groth, D., Mehlhorn, I., Huang, Z., Fletterick, R. J., Cohen, F. E., et al. (1993) Conversion of α-helices into β-sheets features in the formation of the scrapie prion proteins, *Proc. Natl. Acad. Sci. U.S.A. 90*, 10962−10966.
12. Safar, J., Roller, P. P., Gajdusek, D. C., and Gibbs, C. J., Jr. (1993) Thermal stability and conformational transitions of scrapie amyloid (prion) protein correlate with infectivity, *Protein Sci. 2*, 2206−2216.
13. Prusiner, S. B. (1982) Novel proteinaceous infectious particles cause scrapie, *Science 216*, 136−144.
14. Castilla, J., Saa, P., Hetz, C., and Soto, C. (2005) *In vitro* generation of infectious scrapie prions, *Cell 121*, 195−206.
15. Tanaka, M., Chien, P., Naber, N., Cooke, R., and Weissman, J. S. (2004) Conformational variations in an infectious protein determine prion strain differences, *Nature 428*, 323−328.
16. King, C. Y., and Diaz-Avalos, R. (2004) Protein-only transmission of three yeast prion strains, *Nature 428*, 319−323.
17. Chien, P., Weissman, J. S., and DePace, A. H. (2004) Emerging principles of conformation-based prion inheritance, *Annu. Rev. Biochem. 73*, 617−656.
18. Kong, Q., Surewicz, W. K., Petersen, R. B., Zou, W., Chen, S. G., Gambetti, P., Parchi, P., Capellari, S., Goldfarb, L., Montagna, P., et al. (2004) 2nd ed., Cold Spring Harbor Laboratory Press, Cold Spring Harbor, NY.
19. Baker, H. E., Poulter, M., Crow, T. J., Frith, C. D., Lofthouse, R., and Ridley, R. M. (1991) Amino acid polymorphism in human prion protein and age at death in inherited prion disease, *Lancet 337*, 1286.
20. Collinge, J., Palmer, M. S., and Dryden, A. J. (1991) Genetic predisposition to iatrogenic Creutzfeldt−Jakob disease, *Lancet 337*, 1441−1442.
21. Hill, A. F., Desbruslais, M., Joiner, S., Sidle, K. C., Gowland, I., Collinge, J., Doey, L. J., and Lantos, P. (1997) The same prion strain causes vCJD and BSE, *Nature 389*, 448−450, 526.
22. Wadsworth, J. D., Asante, E. A., Desbruslais, M., Linehan, J. M., Joiner, S., Gowland, I., Welch, J., Stone, L., Lloyd, S. E., Hill, A. F., Brandner, S., and Collinge, J. (2004) Human prion protein with valine 129 prevents expression of variant CJD phenotype, *Science 306*, 1793−1796.
23. Goldfarb, L. G., Petersen, R. B., Tabaton, M., Brown, P., LeBlanc, A. C., Montagna, P., Cortelli, P., Julien, J., Vital, C., Pendelbury, W. W., et al. (1992) Fatal familial insomnia and familial Creutzfeldt−Jakob disease: Disease phenotype determined by a DNA polymorphism, *Science 258*, 806−808.
24. Morillas, M., Swietnicki, W., Gambetti, P., and Surewicz, W. K. (1999) Membrane environment alters the conformational structure of the recombinant human prion protein, *J. Biol. Chem. 274*, 36859−36865.

25. Zahn, R., von Schroetter, C., and Wuthrich, K. (1997) Human prion proteins expressed in *Escherichia coli* and purified by high-affinity column refolding, *FEBS Lett. 417*, 400−404.
26. Vanik, D. L., and Surewicz, W. K. (2002) Disease-associated F198S mutation increases the propensity of the recombinant prion protein for conformational conversion to scrapie-like form, *J. Biol. Chem. 277*, 49065−49070.
27. Naiki, H., Higuchi, K., Hosokawa, M., and Takeda, T. (1989) Fluorometric determination of amyloid fibrils *in vitro* using the fluorescent dye, thioflavin T1, *Anal. Biochem. 177*, 244−249.
28. Surewicz, W. K., and Mantsch, H. H. (1988) New insight into protein secondary structure from resolution-enhanced infrared spectra, *Biochim. Biophys. Acta 952*, 115−130.
29. Kad, N. M., Myers, S. L., Smith, D. P., Smith, D. A., Radford, S. E., and Thomson, N. H. (2003) Hierarchical assembly of β2-microglobulin amyloid *in vitro* revealed by atomic force microscopy, *J. Mol. Biol. 330*, 785−797.
30. Santoro, M. M., and Bolen, D. W. (1988) Unfolding free energy changes determined by the linear extrapolation method. 1. Unfolding of phenylmethanesulfonyl α-chymotrypsin using different denaturants, *Biochemistry 27*, 8063−8068.
31. Apetri, A. C., and Surewicz, W. K. (2002) Kinetic intermediate in the folding of human prion protein, *J. Biol. Chem. 277*, 44589−44592.
32. Wildegger, G., Liemann, S., and Glockshuber, R. (1999) Extremely rapid folding of the C-terminal domain of the prion protein without kinetic intermediates, *Nat. Struct. Biol. 6*, 550−553.
33. Swietnicki, W., Morillas, M., Chen, S. G., Gambetti, P., and Surewicz, W. K. (2000) Aggregation and fibrillization of the recombinant human prion protein huPrP90−231, *Biochemistry 39*, 424−431.
34. Morillas, M., Vanik, D. L., and Surewicz, W. K. (2001) On the mechanism of α-helix to β-sheet transition in the recombinant prion protein, *Biochemistry 40*, 6982−6987.
35. Baskakov, I. V., Legname, G., Baldwin, M. A., Prusiner, S. B., and Cohen, F. E. (2002) Pathway complexity of prion protein assembly into amyloid, *J. Biol. Chem. 277*, 21140−21148.
36. Jackson, G. S., Hosszu, L. L., Power, A., Hill, A. F., Kenney, J., Saibil, H., Craven, C. J., Waltho, J. P., Clarke, A. R., and Collinge, J. (1999) Reversible conversion of monomeric human prion protein between native and fibrilogenic conformations, *Science 283*, 1935−1937.
37. Baskakov, I. V. (2004) Autocatalytic conversion of recombinant prion proteins displays a species barrier, *J. Biol. Chem. 279*, 7671−7677.
38. Harper, J. D., and Lansbury, P. T., Jr. (1997) Models of amyloid seeding in Alzheimer's disease and scrapie: Mechanistic truths and physiological consequences of the time-dependent solubility of amyloid proteins, *Annu. Rev. Biochem. 66*, 385−407.
39. Surewicz, W. K., Mantsch, H. H., and Chapman, D. (1993) Determination of protein secondary structure by Fourier transform infrared spectroscopy: A critical assessment, *Biochemistry 32*, 389−394.
40. Zandomeneghi, G., Krebs, M. R., McCammon, M. G., and Fandrich, M. (2004) FTIR reveals structural differences between native β-sheet proteins and amyloid fibrils, *Protein Sci. 13*, 3314−3321.
41. Liemann, S., and Glockshuber, R. (1999) Influence of amino acid substitutions related to inherited human prion diseases on the thermodynamic stability of the cellular prion protein, *Biochemistry 38*, 3258−3267.
42. Hosszu, L. L., Jackson, G. S., Trevitt, C. R., Jones, S., Batchelor, M., Bhelt, D., Prodromidou, K., Clarke, A. R., Waltho, J. P., and Collinge, J. (2004) The residue 129 polymorphism in human prion protein does not confer susceptibility to Creutzfeldt−Jakob disease by altering the structure or global stability of PrPC, *J. Biol. Chem. 279*, 28515−28521.
43. Apetri, A. C., and Surewicz, W. K. (2003) Atypical effect of salts on the thermodynamic stability of human prion protein, *J. Biol. Chem. 278*, 22187−22192.
44. Apetri, A. C., Surewicz, K., and Surewicz, W. K. (2004) The effect of disease-associated mutations on the folding pathway of human prion protein, *J. Biol. Chem. 279*, 18008−18014.
45. Cohen, F. E., Pan, K. M., Huang, Z., Baldwin, M., Fletterick, R. J., and Prusiner, S. B. (1994) Structural clues to prion replication, *Science 264*, 530−531.
46. Swietnicki, W., Petersen, R. B., Gambetti, P., and Surewicz, W. K. (1998) Familial mutations and the thermodynamic stability of the recombinant human prion protein, *J. Biol. Chem. 273*, 31048−31052.
47. Frankenfield, K. N., Powers, E. T., and Kelly, J. W. (2005) Influence of the N-terminal domain on the aggregation properties of the prion protein, *Protein Sci. 14*, 2154−2166.
48. Tahiri-Alaoui, A., and James, W. (2005) Rapid formation of amyloid from α-monomeric recombinant human PrP *in vitro*, *Protein Sci. 14*, 942−947.
49. Riek, R., Wider, G., Billeter, M., Hornemann, S., Glockshuber, R., and Wuthrich, K. (1998) Prion protein NMR structure and familial human spongiform encephalopathies, *Proc. Natl. Acad. Sci. U.S.A. 95*, 11667−11672.
50. Zuegg, J., and Gready, J. E. (1999) Molecular dynamics simulations of human prion protein: Importance of correct treatment of electrostatic interactions, *Biochemistry 38*, 13862−13876.
51. Barducci, A., Chelli, R., Procacci, P., and Schettino, V. (2005) Misfolding pathways of the prion protein probed by molecular dynamics simulations, *Biophys. J. 88*, 1334−1343.
52. Alonso, D. O., DeArmond, S. J., Cohen, F. E., and Daggett, V. (2001) Mapping the early steps in the pH-induced conformational conversion of the prion protein, *Proc. Natl. Acad. Sci. U.S.A. 98*, 2985−2989.
53. Zahn, R., Liu, A., Luhrs, T., Riek, R., von Schroetter, C., Lopez Garcia, F., Billeter, M., Calzolai, L., Wider, G., and Wuthrich, K. (2000) NMR solution structure of the human prion protein, *Proc. Natl. Acad. Sci. U.S.A. 97*, 145−150.
54. Zhang, Y., Swietnicki, W., Zagorski, M. G., Surewicz, W. K., and Sonnichsen, F. D. (2000) Solution structure of the E200K variant of human prion protein. Implications for the mechanism of pathogenesis in familial prion diseases, *J. Biol. Chem. 275*, 33650−33654.
55. Calzolai, L., and Zahn, R. (2003) Influence of pH on NMR structure and stability of the human prion protein globular domain, *J. Biol. Chem. 278*, 35592−35596.
56. Shamsir, M. S., and Dalby, A. R. (2005) One gene, two diseases, and three conformations: Molecular dynamics simulations of mutants of human prion protein at room temperature and elevated temperatures, *Proteins 59*, 275−290.
57. Caughey, B., Raymond, G. J., and Bessen, R. A. (1998) Strain-dependent differences in β-sheet conformations of abnormal prion protein, *J. Biol. Chem. 273*, 32230−32235.
58. Petersen, R. B., Parchi, P., Richardson, S. L., Urig, C. B., and Gambetti, P. (1996) Effect of the D178N mutation and the codon 129 polymorphism on the metabolism of the prion protein, *J. Biol. Chem. 271*, 12661−12668.
59. Tahiri-Alaoui, A., Gill, A. C., Disterer, P., and James, W. (2004) Methionine 129 variant of human prion protein oligomerizes more rapidly than the valine 129 variant: Implications for disease susceptibility to Creutzfeldt−Jakob disease, *J. Biol. Chem. 279*, 31390−31397.
60. Baskakov, I., Disterer, P., Breydo, L., Shaw, M., Gill, A., James, W., and Tahiri-Alaoui, A. (2005) The presence of valine at residue 129 in human prion protein accelerates amyloid formation, *FEBS Lett. 579*, 2589−2596.

BI051455+